Int. J. Electrochem. Sci., 10 **(2015)** 7478 - 7492

International Journal of
ELECTROCHEMICAL
SCIENCE
www.electrochemsci.org

Influence of Anodization Current Density on Preparation and Corrosion of n-Type Macroporous Silicon in 1.0 M NaOH

Chuan Lai[1,2,3,4], *Bin Xie*[2,3,4*], *Like Zou*[3,4], *Yulong Li*[3,4], *Jian Wei*[3]

[1] School of Chemistry and Chemical Engineering, Sichuan University of Arts and Science, Dazhou 635000, PR China
[2] Material Corrosion and Protection Key Laboratory of Sichuan Province, Sichuan University of Science and Engineering, Zigong 643000, PR China
[3] Institute of Functional Materials, Sichuan University of Science and Engineering, Zigong 643000, PR China
[4] Key Laboratory of Green Catalysis of Sichuan Institutes of Higher Education, Sichuan University of Science and Engineering, Zigong 643000, PR China
[*]E-mail: xiebinsuse@126.com

Received: 1 April 2015 / *Accepted:* 2 July 2015 / *Published:* 28 July 2015

The n-type macroporous silicon samples were prepared by electrochemical anodization of n-type silicon wafers in etching solution of HF(40%):EtOH(99.5%)=1:1 with different current density for 20 min. The dissolution of n-type silicon wafers in etching solution conform Faraday's laws of electrolysis. The fabricated n-type macroporous silicon with different porosity and thickness corrosion in 1.0 M NaOH was systemically studied by weight loss measurements, potentiodynamic polarization measurements and scanning electron microscope. Results show that the corrosion rate of n-type macroporous silicon in 1.0 M NaOH increases with anodization current density and porosity increasing, respectively. In addition, the increase of corrosion rate for n-type macroporous silicon prepared with relative higher anodization current density was determined by the activation energy.

Keywords: Microporous materials; Etching; SEM; Corrosion.

1. INTRODUCTION

Porous silicon(PS) was first observed by Uhlir at Bell Labs in 1956 [1]. Owing to the various potential applications in electronics and optoelectronics fields, PS has attracted considerable attention since the observation of its highly efficient visible photoluminescence at room temperature by Canham in 1990 [2]. As a result, the fabrication methods, morphologies, microstructures and optoelectronic properties of PS have been widely studied over the past two decades.

At present, with numerous unique features, such as the high specific surface area, significant optical properties and electronic properties, biocompatibility, biodegradability, bioresorbability and low toxicity, convenient surface chemistry, etc, the PS has applied in electronics, photonics and biosensing [3-7], and been used for an insulating layer in the SOI (silicon-on-insulator) [8-9], a sensing layer in biosensors [9] or chemical sensors [10], an energy carrier [11], a sacrificial layer in micromachining [12], as an important material for solar cell [13], as an excellent biomaterial in tissue engineering, tumor imaging, bioreactor platform drug delivery [3,7]. However, there are few works focusing on researching about the applications of PS in alkaline solutions resulting from the dissolution and corrosion of PS in these solutions [14-16].

The properties, such as porosity, thickness, pore diameter and microstructure of PS, depend on anodization conditions for preparation of PS. The anodization current density is the one of the key condition for PS preparation [17], which can significantly affect the porosity and pore diameters of PS. Based on the size of pore diameters, the fabricated PS can be divided into microporous silicon($\leq$2 nm), mesoporous silicon(2-50 nm) and macroporous silicon($>$50 nm). According to our previous works [18-20], although the corrosion of PS in NaOH, KOH and $(CH_3)_4NOH$ was studied, the anodization current density which acts as a key property for preparation n-type macroporous silicon on their corrosion behavior in alkaline solution, has not been investigated.

Considering the importance of anodization current density on fabrication of PS with different porosity, the aim of this work is to report the effect of anodization current density on preparation and corrosion of n-type macroporous silicon in 1.0 M NaOH. Firstly, several macroporous silicon samples with different porosity were fabricated at various anodization current densities. The mass change of n-type silicon wafers dissolution for preparation n-type macroporous silicon was investigated by gravimetric measurements. Then the corrosion behavior of prepared n-type macroporous silicon in 1.0 M NaOH was systemically investigated by weight loss measurements, potentiodynamic polarization measurements and scanning electron microscope (SEM).

2. EXPERIMENTAL DETAILS

2.1 Reagents and materials

Hydrofluoric acid (40%, A. R., HF), ethanol (99.5%, A. R.), acetone (A. R.) and sodium hydroxide (A. R., NaOH), were purchased from Sinopharm Chemical Reagent Co., Ltd. All the reagents in this work were commercially available and used without further purification. The silicon substrate of silicon wafers was purchased from Emei Semiconductor Material Institute (China), which was a phosphorus doped n-type wafer with a resistivity of 2-4 Ω cm, 500-550 μm thick and (100) oriented.

2.2 Preparation of n-type macroporous silicon

The n-type macroporous silicon samples were prepared by electrochemical anodization of n-type silicon wafers in the etching solution of HF(40%):EtOH(99.5%)=1:1(volume ratio) with different

current densities for 20 min [21-23]. The etching process was performed in a Teflon cell by using two-electrode configuration with Pt gauze as the cathode and silicon substrate as the anode. Meanwhile, the anodization process was illuminated by a 150 W high pressure mercury lamp at a distance of 20 cm. After preparation, the fresh samples were rinsed with double distilled water and ethanol. The most accepted model for describing the etching mechanism of porous silicon preparation had been proposed by Lehmann [24]. In addition, the reaction of silicon etching to prepare porous silicon is given in Eq. (1) [25], where h^+ and e^- represent hole and electron respectively.

$$Si+6HF+2h^+ \longrightarrow H_2+SiF_6^{2-}+4H^++e^- \quad (1)$$

Because of the pore diameter more than 50 nm, the prepared porous silicon turns out to be n-type macroporous silicon.

2.3 Gravimetric measurements

The porosity and thickness of n-type macroporous silicon were usually estimated by gravimetric measurements according to Eq. (2) and (3) [26], where m_1 and m_2 are the mass of the n-type macroporous silicon sample before and after formation and m_3 is the mass of the n-type macroporous silicon sample after porous layer was completely removed by corrosion solution, ρ is the density of silicon and A is the area of the n-type macroporous silicon layer. Gravimetric measurements were carried out in 250 mL beaker with 100 mL 1.0 M NaOH with 20% ethanol (1.0 M NaOH/20% EtOH) acting as optimized corrosion solution at 318 K [26].

$$Porosity\ (\%) = \frac{m_1-m_2}{m_1-m_3} \times 100 \quad (2)$$

$$Thickness = \frac{m_1-m_3}{\rho A} \quad (3)$$

2.4 X-ray diffraction

The microstructure of n-type macroporous silicon was analyzed by X-ray diffraction (XRD-6000, Shimadzu Inc., Japan) equipment operated at 40 kV and 100 mA with Cu Kα at a scanning rate of 5 ° min^{-1}.

2.5 Weight loss measurements

Weight loss measurements were carried out in 250 mL beaker with 100 mL 1.0 M NaOH at different temperatures. The various temperatures were controlled by water thermostat, and all the test solutions were open to air. The mass of cleaned and dried n-type macroporous silicon samples before and after corrosion in the test corrosion solutions were determined by an analytical balance. After weighted, three parallel n-type macroporous silicon samples were immersed in a beaker with the test solutions for different time, which were defined as immersion time. After corrosion, the immersed samples were rinsed thoroughly with double distilled water, ethanol and acetone successively. Then all the samples were dried and re-weighed accurately. Meanwhile, the triplicate experiments were

performed in each case and the mean value of the weight loss was calculated and used to following analysis. The corrosion rate (v) was obtained according to Eq. (4) [18, 19, 20]:

$$v = \frac{m_I - m_{II}}{St} = \frac{\Delta m}{St} \quad (4)$$

where m_I and m_{II} are the mass of the n-type macroporous silicon before and after corrosion. t is the immersion time and Δm is the mass change of the n-type macroporous silicon before and after corrosion for different time, S is the total surface area of the n-type porous layer, which is 0.95 cm^2.

2.6 Potentiodynamic polarization measurements

Potentiodynamic polarization measurements was carried out by a conventional three-electrode cell that consisted of the n-type macroporous silicon working electrode (0.95 cm^2), a silver-silver chloride (Ag/AgCl) electrode as a reference electrode and a platinum gauze as a counter electrode. The measurements was carried out using a computer to control CHI 660b Electrochemical Workstation (China) to investigate the electrochemical behavior of n-type macroporous silicon in 1.0 M NaOH. All the polarization curves were obtained in the potential range of -250 mV to +250 mV in regard to open circuit potential, and the potential sweep rate was 0.5 mV s^{-1}.

In this study, it should be noted that the electrochemical behavior of n-type macroporous silicon in 1.0 M NaOH was investigated at a relative lower temperature of 288 K due to the existence of plenty of bubbles formed from the n-type macroporous silicon in 1.0 M NaOH at the relative higher temperature (above 298 K), which would affect the accuracy of measurements. In addition, the n-type macroporous silicon prepared by electrochemical anodization of n-type silicon wafers in the etching solution of HF(40%):EtOH(99.5%)=1:1 with various anodization current densities was defined as different n-type macroporous silicon.

2.7 Scanning electron microscope

The morphology images of different n-type macroporous silicon before and after corrosion in 1.0 M NaOH at 318 K were investigated by JSM-6510 scanning electron microscope (JEOL) with accelerating voltages of 20 kV, and the working distance of 9-12 mm.

3. RESULTS AND DISCUSSION

3.1 Porosity and thickness

The porosity and thickness of macroporous silicon can be easily estimated using gravimetric measurements by Eq (2) and Eq (3) [27-29]. According to gravimetric measurements, the relationships between mass-change$_{1\text{-}2}$ (m_1-m_2), mass-change$_{1\text{-}2}$ (m_1-m_3) and anodization current density at anodization time of 20 min were shown in Fig. 1.

The mass-change$_{1\text{-}2}$ (m_1-m_2) is the weight loss before and after n-type macroporous silicon formation, which depends on anodization conditions. With fixed etching solution, anodization time,

wafer type, resistivity, illumination, temperature, ambient humidity and drying conditions, the m_1-m_2 linearly increases with anodization current density (J) increasing. The result indicates that the dissolution of n-type silicon wafer conform Faraday's laws of electrolysis (R=0.9993), and the m_1-m_2 of n-type silicon wafers can be calculated by the equation of (m_1-m_2=-0.00143+ 2.146×10^{-4}·J) during the preparation of n-type macroporous silicon by electrochemical anodization.

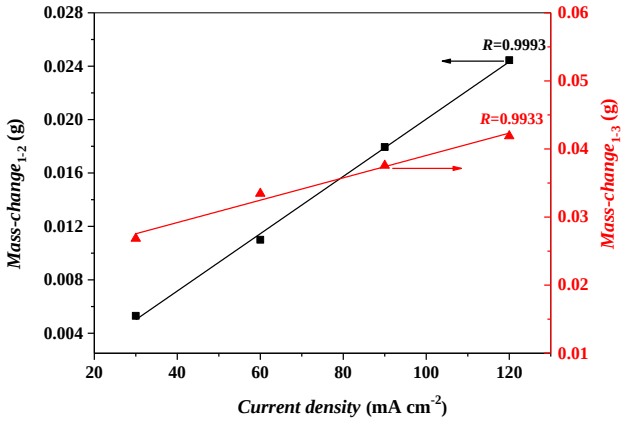

Figure 1. The relationships between mass-change$_{1\text{-}2}$ (m_1-m_2), mass-change$_{1\text{-}3}$ (m_1-m_3) and anodization current density at anodization time of 20 min for n-type macroporous silicon preparation

Moreover, the mass-change$_{1\text{-}3}$ (m_1-m_3) is the total weight loss of the n-type macroporous silicon before formation and after porous layer was completely rapidly removed by 1.0 M NaOH with 20% ethanol acting as an optimized solution [26]. For the constant anodization time of 20 min, the larger the anodization current density is, the higher the m_1-m_3 becomes. As can be seen from Fig. 1, the m_1-m_3 also linearly increases with the increasing anodization current density in the range of 30 mA cm^{-2} to 120 mA cm^{-2}.

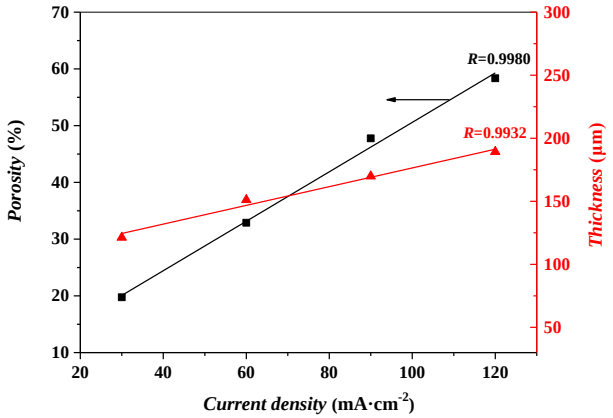

Figure 2. The relationships between porosity, thickness and anodization current density at anodization time of 20 min

Based on Eq. (2) and Fig 1, the porosity and thickness of n-type macroporous silicon prepared at different anodization current densities (J) for 20 min were shown in Fig. 2. It can be clearly seen that the anodization current density has a significant effect on porosity and thickness of n-type macroporous silicon. For fixed anodization time, the porosity increases with anodization current density increasing. The linear fitting results indicate that the porosity and thickness can be given by $porosity(\%)=7.005+0.4357 \cdot J$ and $thickness(\mu m)=102.2+0.7425 \cdot J$ for different n-type macroporous silicon. The porosity of obtained n-type macroporous silicon at anodization current density of 30, 60, 90 and 120 mA cm^{-2} are 19.74%, 32.89%, 47.76%, and 58.35%, respectively. The thickness and porosity are the macroscopic parameters to help in discussing trends but which do not give microscopic information on the morphology of the n-type macroporous silicon layers [30].

3.2 XRD analysis

Fig. 3 (a) and (b) showed the XRD patterns of n-type macroporous silicon prepared on n-type silicon wafers using electrochemical anodization with the anodization current density of 10, 30, 60 and 120 mA cm^{-2} for 20 min.

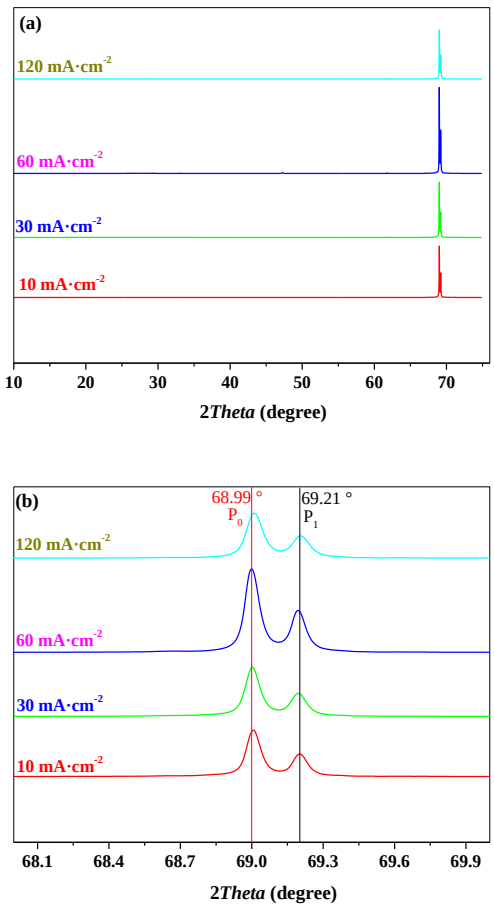

Figure 3. The XRD patterns of n-type macroporous silicon prepared with the anodization current density of 10, 30, 60 and 120 mA cm^{-2} at 20 min

Table 1. The XRD parameters of n-type macroporous silicon prepared with the anodization current density of 10, 30, 60 and 120 mA cm^{-2} at 20 min

Parameters	Current density (mA cm^{-2})			
	10	30	60	120
2θ (°)	69.20560	69.19816	69.18384	69.20560
Intensity (a.u.)	899925	935139	1587885	872229
FWHM (°)	0.06353	0.07784	0.08031	0.08871
D (nm)	121.3	98.96	95.81	86.89

It is observed from Fig. 3 that the presence of two peaks with $2\theta \approx 68.99$ ° (P_0) and 69.21 ° (P_1) are observed for all n-type macroporous silicon samples. The dominant peak (P_0) at about 68.99 ° corresponds to the reflections from (4 0 0) set of planes (JCPDS File No. 89-2955) and is due to crystalline silicon substrate. Another trivial peak (P_1) at about 69.21° is due to the n-type porous layer [30]. The full width at half maximum (FWHM, β) decreases with increasing anodization current density (10-120 mA cm^{-2}). It is observed that the intensity of the peak increases with increasing anodization current density (10-60 mA cm^{-2}). Meanwhile, the intensity of the peak for 120 mA cm^{-2} is lower than it for 60 mA cm^{-2}, which is due to the porous layer falling off the n-type macroporous silicon sample [30].

The grain size (D) of the n-type macroporous silicon was obtained by the Debye-Scherer's formula of ($D = k\lambda/\beta \mathrm{COS}\theta$). Smaller value of FWHM is the indication of good crystallinity and larger grain size of silicon particles. The grain size decrease from 121.3 nm to 86.89 nm is due to the increase of the porosity of n-type macroporous silicon as shown by porosity and SEM analysis.

3.3 Corrosion rate

According to weight loss measurements, the corrosion rate of n-type macroporous silicon in 1.0 M NaOH at different temperatures could be obtained by Eq. (4). The relationships between mass change ($\Delta m/S$) and immersion time for different n-type macroporous silicon corrosion in 1.0 M NaOH were illustrated in Fig. 4 (a), which indicate that the mass change increases with the immersion time increasing. All curves present better linear relationships (R>0.9928) between mass change and immersion time. Based on Eq. (4), the straight slopes (K) and corrosion rate were obtained and listed in Table 2. Meanwhile, the effect of anodization current density on corrosion rate was shown in Fig. 4 (b). From Fig. 4 (b), it can be found that the corrosion rate linearly increases with the anodization current density increasing (R=0.9954).

The essence of n-type macroporous silicon corrosion in 1.0 M NaOH is the reaction among n-type macroporous silicon layer with various Si—H bonds, silicon substrate (Si) with different Si—Si bonds reacting and NaOH aqueous. Besides, the chemical activity of Si—H bonds reacting with NaOH aqueous is higher than the chemical activity of Si—Si bonds [31-33]. Based on the fact, the larger the anodization current density is, the higher the porosity of n-type macroporous silicon becomes, the

more Si—H bonds presence on porous layer, as a result, it can better explain the fact that the corrosion rate increases with anodization current density increasing.

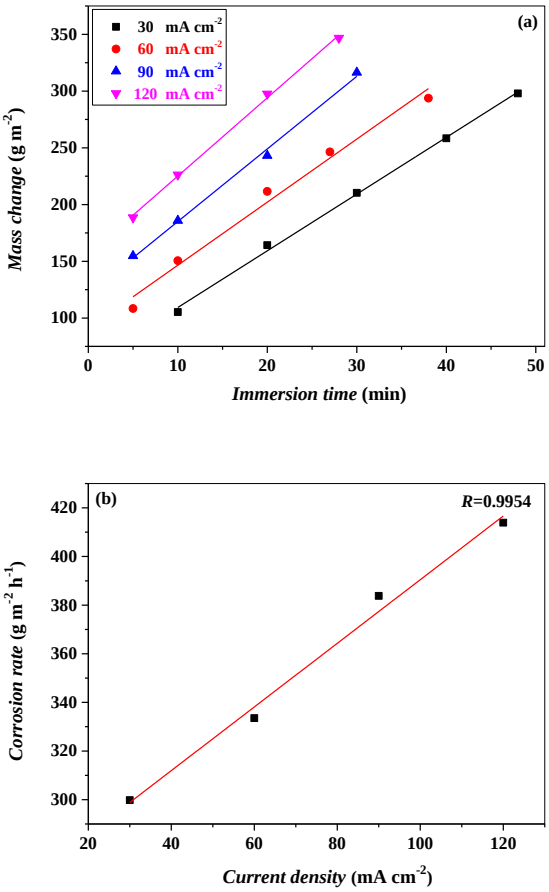

Figure 4. The relationship between mass change and immersion time (a) and relationship between corrosion rate and anodization current density (b) for different n-type macroporous silicon corrosion in 1.0 M NaOH at 318 K

Table 2. The corrosion rate of different n-type macroporous silicon corrosion in 1.0 M NaOH at 318 K

Anodization parameters (x mA cm^{-2}-20 min)	K ($g\ m^{-2}\ min^{-1}$)	v ($g\ m^{-2}\ h^{-1}$)	R
30	4.997	299.8	0.9990
60	5.558	333.5	0.9928
90	6.396	383.8	0.9984
120	6.898	413.9	0.9992

Meanwhile, Fig. 5 presented the effect of temperature on corrosion rate for n-type macroporous silicon prepared with different anodization current densities at 20 min corrosion in 1.0 M NaOH. The result reveals that the corrosion rate increases with temperature increasing, which can be elucidated by Arrhenius equation [18, 20]. Moreover, at the same temperature, the corrosion rate increases with

anodization current density increasing. At 333 K, the corrosion rate of n-type macroporous silicon with a porosity of 58.35% fabricated by anodization current density of 120 mA cm^{-2} is 595.4 g m^{-2} h^{-1}.

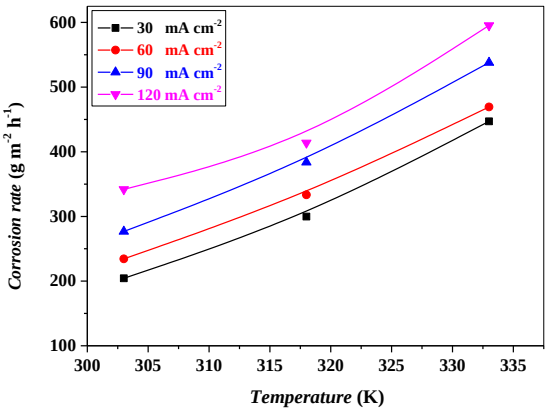

Figure 5. The effect of temperature on corrosion rate for different n-type macroporous silicon corrosion in 1.0 M NaOH

3.6 Potentiodynamic polarization measurements

Fig. 6 showed the potentiodynamic polarization curves for different n-type macroporous silicon corrosion in 1.0 M NaOH at 288 K. According to Fig. 6, the values of corrosion potential (E_{corr}), corrosion current density (I_{corr}), cathodic and anodic Tafel slopes b_c and b_a (V dec^{-1}) obtained and listed in Table 3.

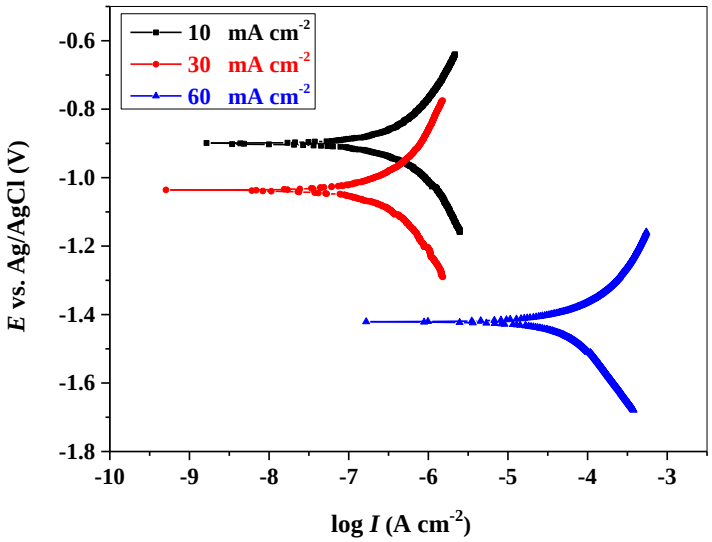

Figure 6. The potentiodynamic polarization curves of different n-type macroporous silicon corrosion in 1.0 M NaOH at 288 K

Table 3. The potentiodynamic polarization parameters of different n-type macroporous silicon corrosion in 1.0 M NaOH at 288 K

Anodization parameters (mA cm^{-2}-20 min)	Porosity (%)	E_{corr} vs. Ag/AgCl (V)	I_{corr} (A cm^{-2})	b_a (V dec^{-1})	b_c (V dec^{-1})
10	11.90	-0.899	3.586×10^{-7}	0.2278	0.2015
30	19.74	-1.036	2.711×10^{-6}	0.2003	0.2180
60	32.89	-1.417	7.524×10^{-5}	0.1796	0.2932

With an inspection of the data in the Table 3, it reveals that the corrosion potential (E_{corr}) shift significantly to more negative potentials with anodization current density and porosity increasing. Besides, the corrosion current density (I_{corr}) remarkably increases with anodization current density and porosity increasing. It's a good agreement between potentiodynamic polarization and weight loss measurements, both of which gave a same trend of n-type macroporous silicon corrosion in 1.0 M NaOH [34].

3.4 Activation parameters

As the essential factors during n-type macroporous silicon corrosion in 1.0 M NaOH, activation parameters (E_a, A, ΔH_a and ΔS_a) were determined by Arrhenius Eq. (5) and transition state Eq. (6) [35-38].

$$\ln v = \ln A - \frac{\Delta E_a}{RT} \quad (5)$$

$$\ln\frac{v}{T} = (\ln\frac{R}{Nh} + \frac{\Delta S_a}{R}) - \frac{\Delta H_a}{RT} \quad (6)$$

where v is the corrosion rate, R is the universal gas constant, h is the Planck's constant, N is the Avogadro's number, T is the absolute temperature, A is the Arrhenius pre-exponential factor, E_a is the activation energy, ΔH_a is the enthalpy of activation and ΔS_a is the entropy of activation.

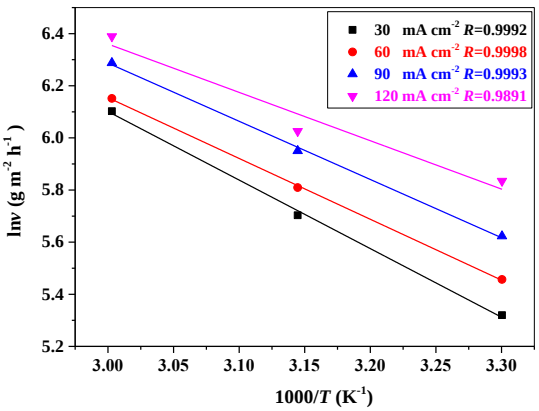

Figure 7. Arrhenius plots for n-type macroporous silicon corrosion in 1.0 M NaOH

Based on weight loss measurements results, the Arrhenius plots of ln$v$ vs. 1000/T and ln(v/T) vs. 1000/T for n-type macroporous silicon with different porosity corrosion in 1.0 M NaOH were shown in Fig. 7 and Fig. 8, respectively. Meanwhile, the calculated values of E_a, A, ΔH_a and ΔS_a were listed in Table 4.

From Fig. 7, the good linear relationships between ln$v$ and 1000/T (R>0.9891) indicates that the corrosion of different n-type macroporous silicon in 1.0 M NaOH can be elucidated by Arrhenius kinetic model. According to Table 4, with the anodization current density increasing, both the activation energy and Arrhenius pre-exponential factor decrease accordingly. Based on Eq. (5), it can be concluded that both the higher Arrhenius pre-exponential factor and the lower activation energy lead to the higher corrosion rate. In this work, the values of Arrhenius pre-exponential factor and activation energy of n-type macroporous silicon with relative low anodization current density were higher than those with relative high anodization current density. Therefore, the increase of corrosion rate for n-type macroporous silicon prepared with high anodization current density was determined by the activation energy (E_a).

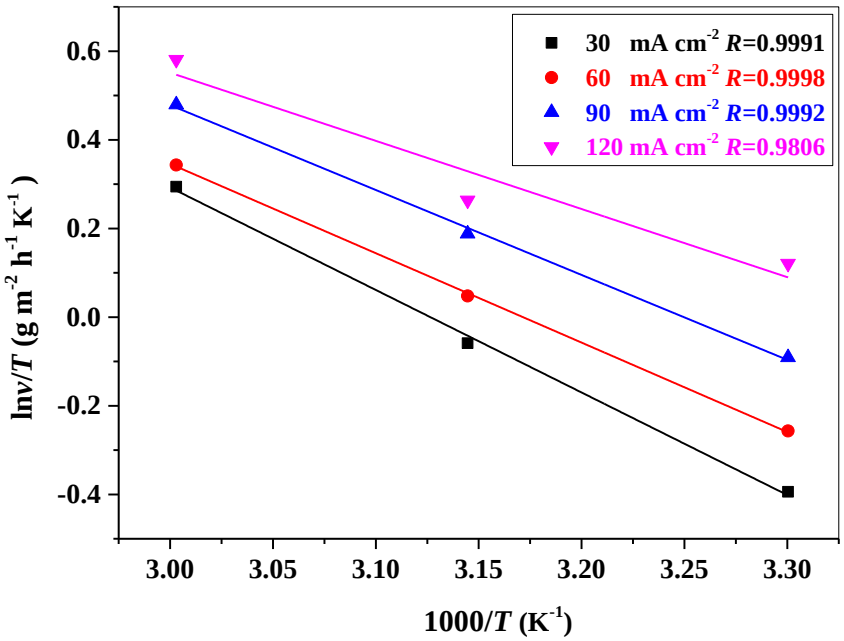

Figure 8. Transition state plots for n-type macroporous silicon corrosion in 1.0 M NaOH

Fig. 8 reveals the relationship between ln (v/T) and 1000/T. Straight lines were obtained with a slope of -ΔH_a/R and an intercept of ln(R/Nh)+ΔS_a/R, from which the enthalpy of activation and entropy of activation were calculated and listed in Table 4. Both the enthalpy of activation and entropy of activation for n-type macroporous silicon prepared with the relative lower anodization current density were higher than that with the relative higher anodization current density.

Table 4. The activation parameters of different n-type macroporous silicon corrosion in 1.0 M NaOH

Anodization parameters (mA cm^{-2}-20 min)	E_a (KJ mol^{-1})	A (g m^{-2} h^{-1})	ΔH_a (KJ mol^{-1})	$-\Delta S_a$ (J K^{-1} mol^{-1})
30	21.87	1.193×10^{6}	19.23	137.4
60	19.41	5.175×10^{5}	16.77	144.4
90	18.57	4.370×10^{5}	15.93	145.8
120	15.42	1.511×10^{5}	12.79	154.6

3.5 Scanning electron microscope

The SEM images of n-type macroporous silicon, prepared with different anodization current density of 30, 60 and 120 mA cm^{-2}, corroded in 1.0 M NaOH at 318 K were shown in Fig. 9 (a-f). The results show that the anodization current density has a significant effect on the morphology and porosity of n-type macroporous silicon. Fig. 9 (a), (c) and (e) are the SEM images of n-type macroporous silicon with different porosity before corrosion. A few pores can be seen on the surface of n-type macroporous silicon prepared at anodization current density of 30 mA cm^{-2} (a) without any cracks. On the contrary, it is clearly seen the cracks on the surface of n-type macroporous silicon prepared at anodization current density of 60 mA cm^{-2} (c) and 120 mA cm^{-2} (e), and with no pores.

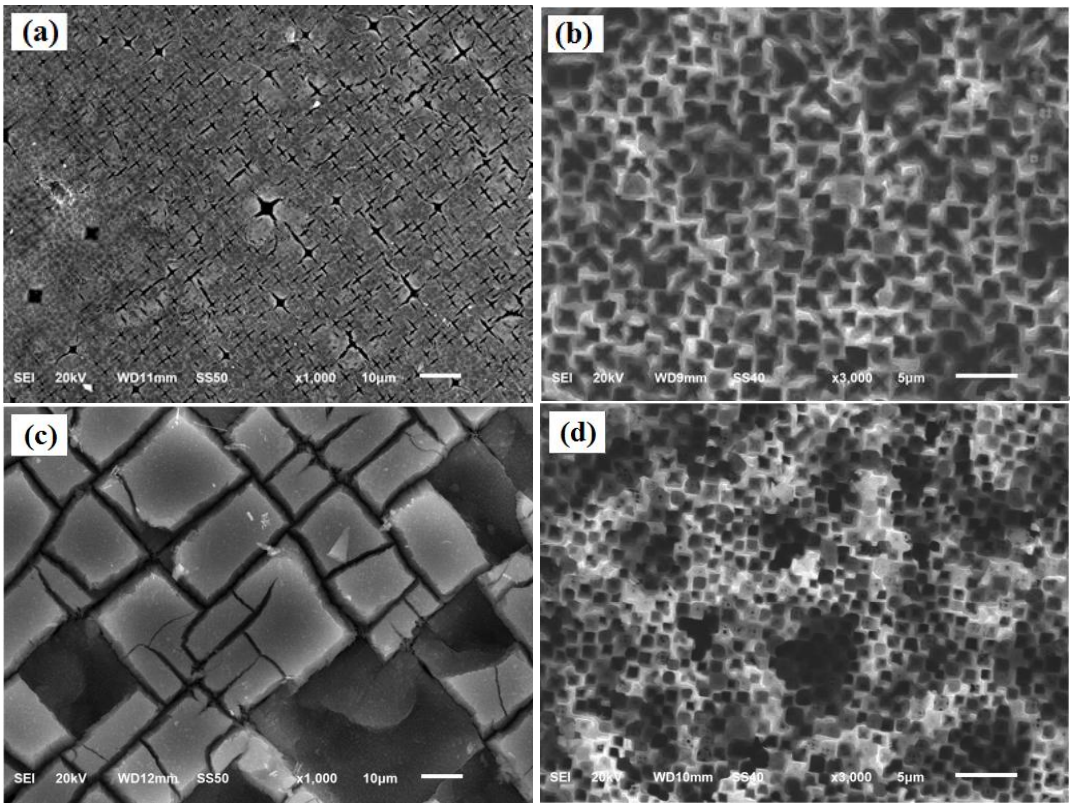

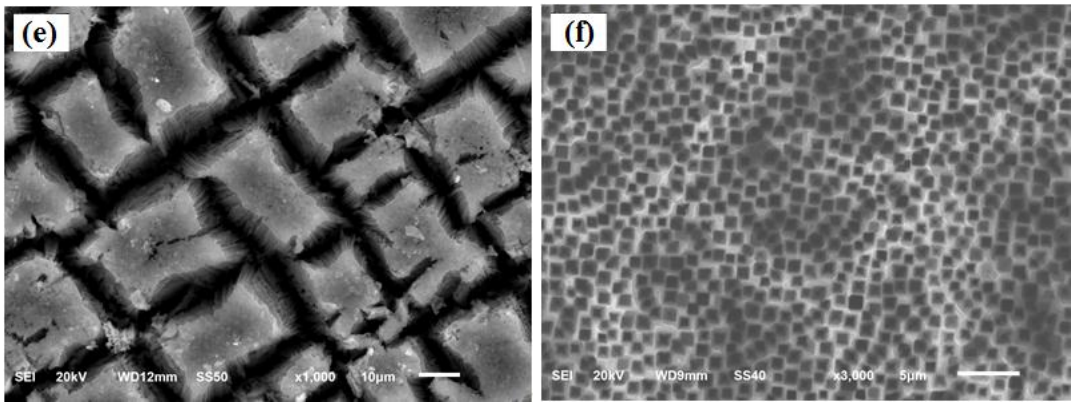

Figure 9. The SEM images of different n-type macroporous silicon before (a, c, e) and after (b, d, f) corrosion in 1.0 M NaOH at 318 K for 10 min

Fig. 9 gives a comparison about the surface microstructures on different n-type macroporous silicon before and after corrosion. Along with the corrosion reaction, as can be seen, all the samples (a, c and e) were seriously damaged and the porous structure (b, d and f) were clearly seen after corrosion in 1.0 M NaOH for 10 min, resulting more pores exposed on the surface of n-type macroporous silicon. The fabricated porous silicon turns out to be n-type macroporous silicon for the average pore diameters of each n-type porous silicon sample of about 1 μm. Compared Fig. 9 (b), Fig. 9 (d) with Fig. 9 (f), the corrosion surface of the n-type macroporous silicon prepared at anodization current density of 30 mA cm^{-2} (b) and 60 mA cm^{-2} (d) suffer from a lack of uniformity with the appearance of heterogeneous pores. On the contrary, after corrosion, the surface of n-type macroporous silicon prepared at anodization current density of 120 mA cm^{-2} (f) shows a uniform porous surface with a higher porosity. The above results confirm that the porosity increases with the anodization current density increasing.

4. CONCLUSIONS

All the n-type macroporous silicon samples were fabricated by electrochemical anodization of n-type silicon wafers in the etching solution of HF(40%):EtOH(99.5%)=1:1. The dissolution of silicon wafers in etching solution for preparing n-type macroporous silicon conform Faraday's laws of electrolysis. The relationships between mass-change$_{1\text{-}2}$ (m_1-m_2), mass-change$_{1\text{-}3}$ (m_1-m_3), porosity, thickness and anodization current density show the good linear relationships, respectively. Corrosion rate of n-type macroporous silicon in 1.0 M NaOH linearly increases with anodization current density and porosity increasing. The corrosion potential shift significantly to more negative potentials and corrosion current density increases as anodization current density increasing. In addition, in 1.0 M NaOH, the activation parameters (E_a, A, ΔH_a and ΔS_a) of n-type macroporous silicon prepared with different anodization current density were obtained. The increase of corrosion rate for n-type macroporous silicon prepared with relative higher anodization current density was determined by activation energy.

ACKNOWLEDGEMENTS
This project is supported by the Opening Project of Material Corrosion and Protection Key Laboratory of Sichuan Province (No 2015CL09), and the Opening Project of Key Laboratory of Green Catalysis of Sichuan Institutes of Higher Education (No LYJ1503).

Reference

1. Uhlir, *Bell Syst. Tech. J.*, 35 (1956) 333.
2. L.T. Canham, *Appl. Phys. Lett.*, 57 (1990) 1046.
3. N.H. Maniya, S.R. Patel and Z.V.P. Murthy, *Mater. Res. Bull.*, 57 (2014) 6.
4. V.S.Y. Lin, K. Motesharei, K.P.S. Dancil, M.J. Sailor and M.R. Ghadiri, *Science*, 278 (1997) 840.
5. F. Cunin, T.A. Schmedake, J.R. Link, Y.Y. Li, J. Koh, S.N. Bhatia and M.J. Sailor, *Nat. Mater.*, 1 (2002) 39.
6. W. Sun, J.E. Puzas, T.J. Sheu, X. Liu and P.M. Fauchet, *Adv. Mater.*, 19 (2007) 921.
7. A. Tzur-Balter, A. Gilbert, N. Massad-Ivanir and E. Segal, *Acta Biomater.*, 9 (2013) 6208.
8. J.D. Benjamin, J.M. Keen, A.G. Cullis, B. Innes and N.G. Chew, *Appl. Phys. Lett.*, 49 (1986) 716.
9. H.Y. Zhang, Z.H. Jia, X.Y Lv, J. Zhou, L.L. Chen, R.X. Liu and J. Ma, *Biosens. Bioelectron.*, 44 (2013) 89.
10. G. Toker, R. Sagi, S.B. Nachum and M. Asscher, *J. Chem. Phys.*, 138 (2013) 044710-1.
11. C.Y. Zhan, P.K. Chu, D. Ren, Y.C. Xin, K.F. Huo,Y. Zou and N.K. Huan, *Int. J. Hydrogen Energy*, 36 (2011) 4513.
12. W. Lang, P. Steiner, A. Richter, K. Marusczyk, G. Weimann and H. Sandmaier, *Sens. Actuators A: Phys.*, 43 (1994) 239.
13. I.I. Ivanov, V.A. Skryshevsky, T. Nychyporuk, M. Lemiti, A.V. Makarov, N.I. Klyui and O.V. Tretyak, *Renew. Energ.*, 55 (2013) 79.
14. Y.Q. Qu, X. Zhong, Y.J. Li, L. Liao, Y. Huang and X.F. Duan, *J. Mater. Chem.*, 20 (2010) 3590.
15. G.L. Liu, P.Y. Dai, Y.Z. Wang, J.F. Yang and Y.B. Zhang, *J. Eur. Ceram. Soc.*, 31 (2011) 847.
16. J. Kanungo, S. Maji, H. Saha and S. Basu, *Mater. Sci. Eng. B*, 167 (2010) 91.
17. K. Rahmoun, H.I. Faraoun, G. Bassou, C. Mathieu and N.E.C. Sari, *Physics Procedia*, 55 (2014) 390.
18. C. Lai, X.M Li, L.K Zou, Q. Chen, B. Xie, Y.L Li, X.L. Li and Z. Tao, *Corros. Sci.*, 85 (2014) 471.
19. C. Lai, X.M Li, Z. Xiang, Z. Tao, D.X. Zhang and W.J. Yang, *Corros. Eng. Sci. Techn.*, 49 (2014) 386.
20. C. Lai, X.M Li, D.X. Zhang, Z. Xiang, W.J. Yang and X.G. Guo, *Mater. Chem. Phys.*, 144 (2014) 355.
21. F.A. Harraz, A.M. Salem, B.A. Mohamed, A. Kandil and I.A. Ibrahim, *App. Surf. Sci.*, 264 (2013) 391.
22. A.G. Cullis, L.T. Canham and P.D.J. Calcott, *J. Appl. Phys.*, 82 (1997) 909.
23. F.A. Harraz, T. Sakka and Y.H. Ogata, *Electrochim. Acta* , 50 (2005) 5340.
24. V. Lehmann and U. Gösele, *Appl. Phys. Lett.*, 58 (1991) 856.
25. S. Dhanekar and S. Jain, *Biosens. Bioelectron.*, 41 (2013) 54.
26. C. Lai, X.M Li, C.L Liu, X.G. Guo,Z. Xiang, B.Xie and L.K.Zou, *Mater. Sci. Semicon. Proc.*, 26 (2014) 501.
27. S. Lazarouk, P. Jaguiro, S. Katsouba, G. Maiello, S. La Monica, G. Masini, E. Proverbio and A. Ferrari, *Thin Solid Films*, 297 (1997) 97.
28. J. Kanungo, S. Maji, H. Saha and S. Basu, *Mater. Sci. Eng. B*, 167 (2010) 91.
29. K. Kordás, J. Remes, S. Beke, T. Hu and S. Leppävuori, *Appl. Surf. Sci.*, 178 (2001) 190.
30. D. Buttard, D. Bellet and T. Baumbach, *Thin Solid Films*, 276 (1996) 69.

31. W.C. Wu, Z.M. Ao, T. Wang, C.L. Li and S.A. Li, *Phys. Chem. Chem. Phys*., 16 (2014) 16588.
32. X.W. Zhou, M. Ishida, A. Imanishi and Y. Nakato, *J. Phys. Chem. B*, 105 (2001) 156.
33. C.J. Wu and E.A. Carter, *Chem. Phys. Lett*., 185 (1991) 171.
34. Z. Xiang, C. L. Liu and C. Lai, *Int. J. Electrochem. Sci.*, 10 (2015) 3935.
35. X.H. Li, S.D Deng and X.G. Xie, *Corros. Sci.*, 81 (2014) 162.
36. X.H. Li, S.D Deng, X.G. Xie and H. Fu, *Corros. Sci.*, 87 (2014) 15.
37. N. Soltani, M. Behpour, S. M. Ghoreishi and H. Naeimi, *Corros. Sci.*, 52 (2010) 1351.
38. P. Mourya, S. Banerjee and M.M. Singh, *Corros. Sci.*, 85 (2014) 352.